PAPER

Unseeded velocimetry in nitrogen for high-pressure, cryogenic wind tunnels: part III. Resonant femtosecond-laser tagging

IOP Publishing Measurement Science and Technology
Meas. Sci. Technol. **31** (2020) 075203 (15pp) https://doi.org/10.1088/1361-6501/ab7bbc

Unseeded velocimetry in nitrogen for high-pressure, cryogenic wind tunnels: part III. Resonant femtosecond-laser tagging

Daniel T Reese[1], **Naibo Jiang**[2] **and Paul Danehy**[1]

[1] NASA Langley Research Center, Hampton, VA 23681, United States of America
[2] Spectral Energies, LLC, Dayton, OH 45430, United States of America

E-mail: daniel.reese@nasa.gov

Received 7 October 2019, revised 13 December 2019
Accepted for publication 2 March 2020
Published 24 April 2020

Abstract

Selective two-photon absorptive resonance femtosecond laser electronic excitation tagging (STARFLEET) velocimetry is characterized for the first time at high-pressure, low-temperature conditions. Studies were carried out in the NASA Langley Research Center's 0.3 meter transonic, cryogenic wind tunnel, with flow conditions spanning the entire operational envelope of the facility; total pressures ranging from 100 kPa to 517 kPa, total temperatures from 80 K to 327 K, and Mach numbers from 0.2 to 0.85. STARFLEET signal intensity and lifetime measurements are examined for their thermodynamic dependencies since both intensity and lifetime have implications for measurement precision. Signal intensity is found to be inversely proportional to density, while lifetime scales nearly linearly with density until approaching the liquid-vapor saturation point of nitrogen. The velocity measurement accuracy and precision are assessed over the full domain of conditions, and standard error was determined to be 1.6%, while precision ranged from roughly 1.5% to 10% of the freestream velocity. The precision was also observed to have a temperature dependence, likely a result of the longer lifetimes experienced at higher densities.

Keywords: femtosecond laser, molecular tagging velocimetry, resonant excitation

(Some figures may appear in color only in the online journal)

1. Introduction

The importance of transonic, cryogenic wind tunnels (TCTs) in aerospace vehicle research and development cannot be overstated. These unique facilities allow for the testing of scaled models at flight-accurate Reynolds numbers, providing valuable information on the aerodynamic effects experienced in-flight. To achieve these large Reynolds numbers—which can be in excess of 4.2×10^8 m^{-1} [1]—TCTs run at high static pressures and low temperatures, which increases flow density while decreasing dynamic viscosity [2–4]. Operating in this extreme environment necessitates rugged construction of the wind tunnel facility and produces a challenging testing environment which is often not amenable to the implementation of measurement techniques—optical measurement techniques in particular. Limited optical access, large vibrations, frost accumulation, and thermal expansion and contraction of the facility are just some of the factors that contribute to the difficulties encountered when making measurements in large-scale TCTs.

Despite the significant challenges associated with testing in high-pressure, cryogenic wind tunnels, several diagnostics have found use in TCTs, albeit to varying levels of success. Measurement techniques such as photogrammetry [5, 6] and Moiré interferometry [7] have been successfully applied in the National Transonic Facility (NTF) and the European Transonic Windtunnel (ETW) to provide aeroelastic deformation measurements on a variety of different models. On-body surface pressures and temperatures have been measured using

cryogenic pressure- and temperature-sensitive paints [8–12]. In the NTF, flow disturbance measurements were made using a survey rake containing various temperature, velocity, and pressure probes; however, the cryogenic environment was found to negatively impact the survivability and repair of hot wire probes [13]. Other off-body measurements that have been successfully employed in TCTs include density-sensitive techniques such as Rayleigh scattering [14–16], schlieren [17], and shadowgraphy [4].

Though many of the aforementioned measurement techniques have seen widespread application across several different cryogenic wind tunnels, the use of optical velocimetry in TCTs remains limited. Techniques such as particle image velocimetry (PIV) [9, 18, 19] and Doppler global velocimetry (DGV) [20] have only seen use in the European TCT facilities of ETW and the cryogenic wind tunnel Cologne (DNW-KKK). While these techniques have been proven to provide two-dimensional, two-component velocity fields in a high-speed, cryogenic flow (including time-resolved measurements of turbulence in the wake of a stalled aircraft wing [21]), these types of measurements are disallowed in the NASA TCT facilities due to their reliance on particle seeding. The introduction of tracer particles is forbidden in NASA's TCTs to prevent damage to sensitive facility components, as well as inhibit abrasive erosion of the tunnel interior and the collection of particles (such as water vapor ice) on test models, which causes surface roughness. Although active particle seeding is prohibited in the TCTs of NASA, two studies have relied on naturally-occurring seed present in the Langley 0.3 m TCT facility in order to carry out laser Doppler velocimetry [22] and laser transit anemometry [23]. Both of these studies found success over a limited range of the tunnel operating conditions, but the seeding methods used were neither repeatable nor consistent, and the source of the seed remained undetermined.

To avoid restrictive operational protocols and other issues associated with particle seeding, one option is to utilize a class of optical velocimetry techniques known as molecular tagging velocimetry (MTV). MTV methods rely on the use of molecules, rather than particles, to act as a tracer. Often times the tracer molecule is naturally present in the test gas (e.g. N_2 in air or nitrogen wind tunnels) and altogether prevents the need to seed the flow; this subclass is known as unseeded MTV. Femtosecond laser electronic excitation tagging (FLEET) [24] is one such unseeded MTV technique, wherein a laser is used to dissociate and ionize molecular nitrogen. The subsequent recombination of nitrogen atoms results in a long-lived (on the order of 10 μs) emission which can be used to track the tagged region of fluid and measure velocity. The pressure dependence of the FLEET signal intensity [25] and the effect of temperature on the FLEET spectrum [26] have also been investigated, and show potential for providing a method of obtaining simultaneous multi-parameter measurements using the technique. Further information about FLEET can be found in references [24, 27] and in part I of this series of papers [28]. Another recently developed unseeded MTV measurement technique (belonging to the same class of optical diagnostics as FLEET) is picosecond laser electronic excitation tagging (PLEET) [29]. PLEET is a high-speed variant of FLEET that utilizes a pulse-burst laser system to make unseeded velocity measurements at up to 100 kHz. Further details regarding PLEET are given in reference [29] and in part II of this series of papers [30].

Yet another variant of FLEET (and the focus of the current work), is selective two-photon absorptive resonant FLEET (STARFLEET) [31]. The STARFLEET technique exploits the resonant excitation of the N_2 $a''^1\sum_g^+ \leftarrow X^1\sum_g^+$ transition [31, 32] via two-photon absorption near 202 nm, which allows for emission intensities similar to FLEET using a small fraction of the laser energy. A number of benefits can be gained by utilizing the resonant nature of STARFLEET. Primarily, while FLEET causes large thermal perturbations on the order of 100 s of K (and PLEET causes an even greater temperature rise), the thermal perturbation accompanying STARFLEET is greatly reduced (on the order of 10 K), minimizing the disturbance of the measurement on the flow of interest and increasing thermometric accuracy [31]. The lower laser energies required by the STARFLEET technique also results in less severe damage to materials such as mirrors, windows, and test models. In addition to the many benefits afforded by the technique, STARFLEET also comes with several drawbacks. The deep-UV wavelength required for resonant excitation necessitates the use of costly windows and focusing optics, and, combined with the ultra-fast nature of the femtosecond pulse, leads to large energy losses at each turning mirror. In spite of these challenges, STARFLEET has been successfully demonstrated at 300 K in the NASA Langley 0.3 m TCT in both the freestream and in the wake behind a cylindrical model [33, 34].

This work serves as the third installment in a series of papers detailing unseeded velocimetry techniques applicable in nitrogen for use in high-pressure, cryogenic wind tunnels. While the first paper [28] covers FLEET, and part II [30] details PLEET, the present paper will characterize the STARFLEET technique. As with the previous two works, the studies described herein were conducted in the NASA Langley 0.3 m TCT and covered conditions spanning the entire operational envelope of the facility. STARFLEET is assessed for accuracy and precision, and the thermodynamic dependencies of the technique are explored. The following section outlines the experimental setup, detailing the wind tunnel facility, laser delivery system used to write the STARFLEET line, and the imaging system used to capture the signal. Section 3 covers a set of fundamental studies conducted to better understand the STARFLEET signal, including the effect of laser energy, excitation wavelength, and the emission spectrum. Data processing (including preprocessing, peak-signal determination, and velocity and signal lifetime calculations) is described in section 4, while section 5 provides experimental results and a discussion. Final conclusions are drawn in section 6.

2. Experimental setup

The experimental setup utilized in these experiments is described in detail in this section. Subsection 2.1 discusses the 0.3 m facility, subsection 2.2 outlines the 'write' system used

to produce and deliver the laser beam to the test section, and subsection 2.3 details the 'read' system that was employed to record the STARFLEET signal.

2.1. Test facility

The NASA Langley 0.3 m transonic cryogenic wind tunnel is a fan-driven, closed-loop wind tunnel capable of operating with air, nitrogen, or sulfur hexafluoride as the test gas [2]. All results presented in this work were conducted in pure nitrogen to allow for the highest Reynolds numbers and optimal performance of the STARFLEET technique. The test section of the wind tunnel has a double-shelled construction, consisting of an outer pressure shell to contain the high pressure experienced during operation, and an inner test section through which the test gas flows. The dimensions inside the test section are 0.33 m $\times$ 0.33 m, and the top and bottom walls are aerodynamically parallel—slightly divergent to account for the growth of the boundary layers. Optical access into the test section was provided through two sets of windows: one pair of quartz (amorphous SiO_2) windows for imaging the STARFLEET signal, and one pair of magnesium fluoride (MgF_2) windows to allow for laser passage.

The wind tunnel is capable of operating at total pressures ranging from 100 kPa to 517 kPa, total temperatures from 80 K to 327 K, and Mach numbers from 0.2 to 0.85 [2]. The 0.3 m TCT facility was equipped with an array of static and total pressure probes, as well as thermocouple probes and strain gauges; collectively known as the data acquisition system (DAS). The DAS recorded and displayed relevant test conditions, and read this data into a network of facility computer systems for processing. Velocities were calculated using the static and total pressure probes, a total temperature probe, and a real-gas equation of state (Beattie-Bridgeman equation) for computing the density of the gas [30]. Each time a STARFLEET measurement was taken, a data point from the facility DAS system was also recorded for validation and verification of the STARFLEET velocity measurement in post-processing.

2.2. Write system

The 'write system' consists of all components necessary to produce and direct the laser beam used to write the STARFLEET line, as well as focus the beam within the measurement region inside the test section. The source of the write system was a regeneratively amplified Ti:sapphire laser system (Spectra-Physics Solstice) with a repetition rate of 1 kHz, a temporal bandwidth of 92 fs, a center wavelength of 807 nm, and a bandwidth of 13 nm. This laser was used as input to a fourth-harmonic generator (FHG) [35] in order to create the 201.75 nm light that was used to write the STARFLEET line. After exiting the FHG, the spectral bandwidth of the frequency-quadrupled beam was approximately 1 nm and was directed to the wind tunnel using a series of remotely-adjustable mirrors. Several of the mirrors were equipped with a camera monitoring the location of the beam on the mirror, which allowed for real-time adjustment and alignment of the beam in order to compensate for any misalignment due to thermal expansion and contraction of the wind tunnel. Once the beam reached the wind tunnel, it penetrated the outer pressure shell through a 5 mm thick MgF_2 window, passed through a 250 mm MgF_2 focusing lens located in the plenum, and entered the test section through a second MgF_2 window located in the test section wall. A schematic showing the experimental setup, including the path of the laser beam, is shown in figure 1.

Although the laser system produced approximately 90 μJ/pulse at the exit of the FHG, only 26 μJ/pulse were present inside of the test section. This drop in energy was caused partially by the UV laser propagating through air, but also from losses incurred at each mirror, focusing optic, and window. Despite only delivering 32.5% of the available laser energy to the test section, the 26 μJ/pulse represents a >3$\times$ increase in delivered energy over previous STARFLEET tests conducted in the same facility [33, 34]. This increase in energy delivered to the test section was obtained through a combination of a 33% increase in output energy from the FHG compared with previous studies, as well as a reduction in the total number of mirrors used to direct the laser beam to the measurement region.

2.3. Read system

The 'read system' records a time series of images of the STARFLEET line created by the write system in order to obtain the raw data used for velocimetry and lifetime measurements. As a result of the spectral study conducted prior to the experimental campaign, STARFLEET emission was recorded using a UV high-speed image intensifier (LaVision HS-IRO with an S20 photocathode and a P46 phosphor screen) lens-coupled to a high-speed CMOS camera (Photron SA-Z). A 100 mm focal length, $f/2$ UV Halle lens was used for imaging the STARFLEET emission, yielding a magnification of 1/8. Given a standoff distance of approximately 0.9 m, the collection solid angle is ~0.0024 sr, resulting in the collection of about 0.02% of the total STARFLEET signal. Signal levels could be increased in future experiments by using an objective lens with a lower f-number and shortening the standoff distance; however, this was not possible in the current campaign due to cost and facility constraints.

The imaging system viewed the STARFLEET signal using a 6.35 cm diameter AR-coated quartz window to penetrate the outer pressure shell, and a second quartz window within the test section wall. An imaging periscope, along with the relative positions of the two quartz windows, afforded the perspective to view the STARFLEET line from above, rather than using the quasi-boresight configuration utilized in many previous experiments carried out in the 0.3 m TCT [28, 30, 36–38]. The read system captured 12 frames of data (with 1 μs exposure every 2.5 μs, corresponding to a rate of 400 kHz) for each run condition. This is twice the time interval captured in earlier STARFLEET experiments [33, 34], which was made possible due to the increased laser energy delivered to the test section. The first frame of each set was a 'cleaning frame'

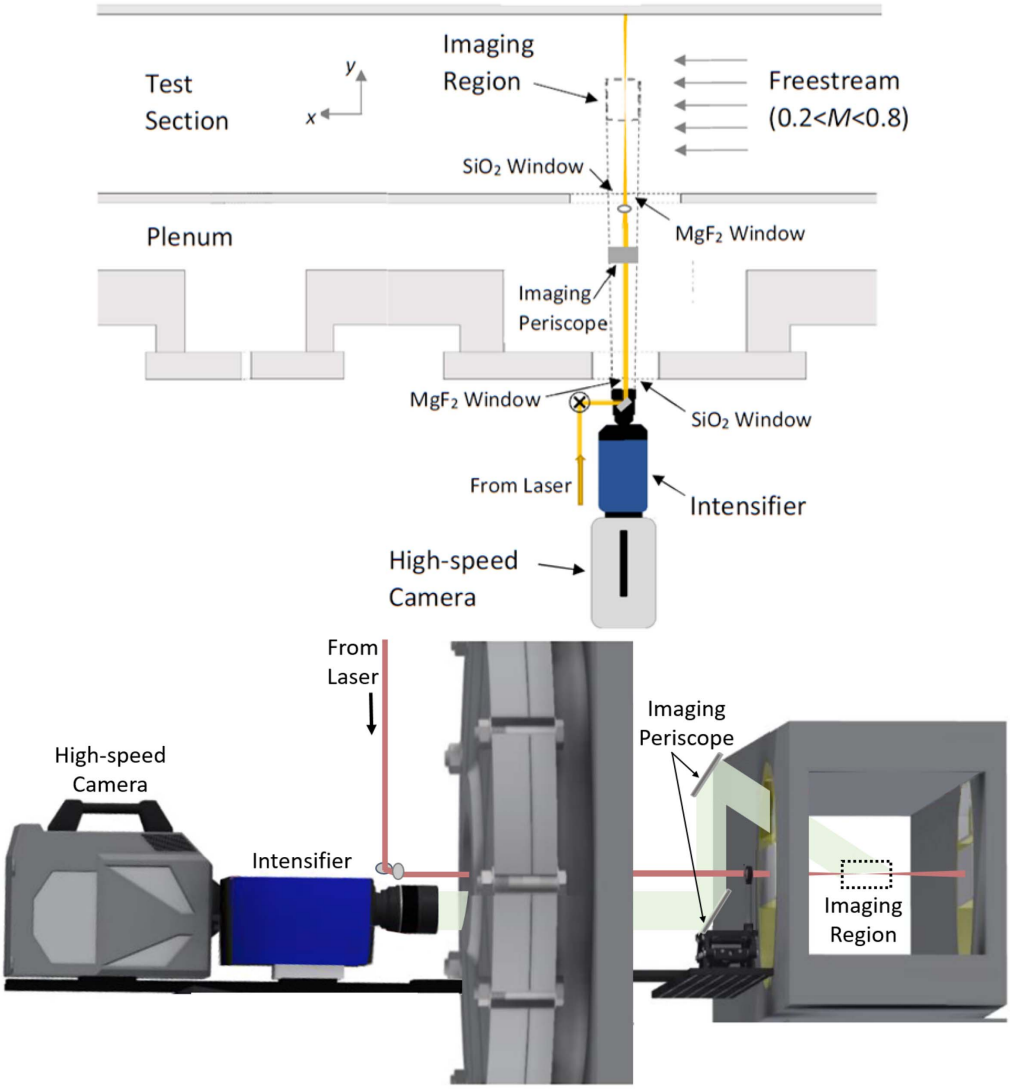

Figure 1. Schematic of imaging and optical setup used in the 0.3 meter TCT for STARFLEET experiments (top—overhead view; bottom—perspective view). The camera views the STARFLEET line from above using the imaging periscope. The MgF_2 and quartz windows are for laser delivery and imaging, respectively.

used to remove unwanted accumulated charge from the cameras detector, the second frame was a background image used in data processing, and the last 10 frames contained the STARFLEET signal at several time delays (with the first frame containing STARFLEET signal occurring 1.2 μs after the laser pulse). While every set contains up to 10 frames of STARFLEET data, there is only one laser pulse per set. Figure 1 shows a schematic of the experimental setup, including the read system.

3. Fundamental studies

Because STARFLEET is a relatively new technique, fundamental studies must be conducted to better understand how the technique behaves and to guide the experimental setup. This is accomplished through three independent studies. First, a wavelength study is conducted to explore the sensitivity of the technique to excitation wavelength of the laser and determine the wavelength corresponding to peak resonance. Next the effect of varying laser excitation energies is explored in section 3.2. Finally, the spectrum of the STARFLEET signal emission is studied in section 3.3 using a spectrometer and a series of Wratten filters.

3.1. Excitation wavelength study

Given that STARFLEET is a resonant technique, it should be relatively sensitive to excitation wavelength. To ensure studies were conducted at peak resonance, the laser beam used to write the STARFLEET line was tuned to seven wavelengths between 201.3 nm and 202.8 nm, and images were taken of the resultant signal. At each wavelength, 400 images are obtained and averaged to provide a corresponding maximum signal intensity. Relative intensity was plotted as a function of wavelength, and results were fit to a Gaussian model in order

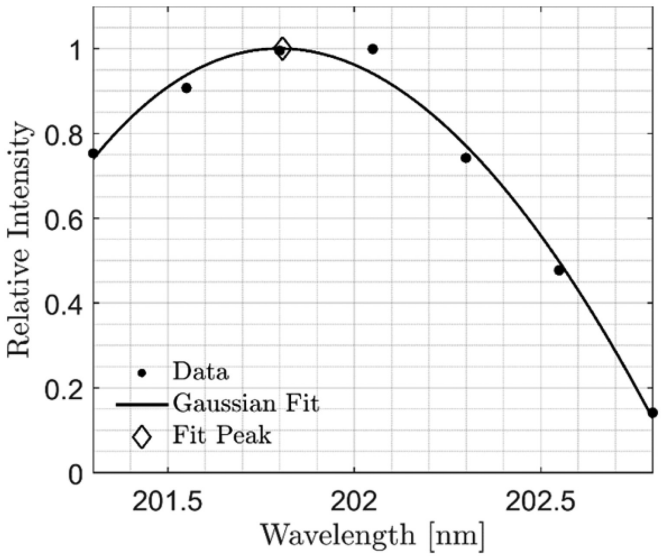

Figure 2. Excitation scan showing the relative STARFLEET signal intensity as a function of laser wavelength. A Gaussian fit to data indicates peak resonance occurs at approximately 201.8 nm.

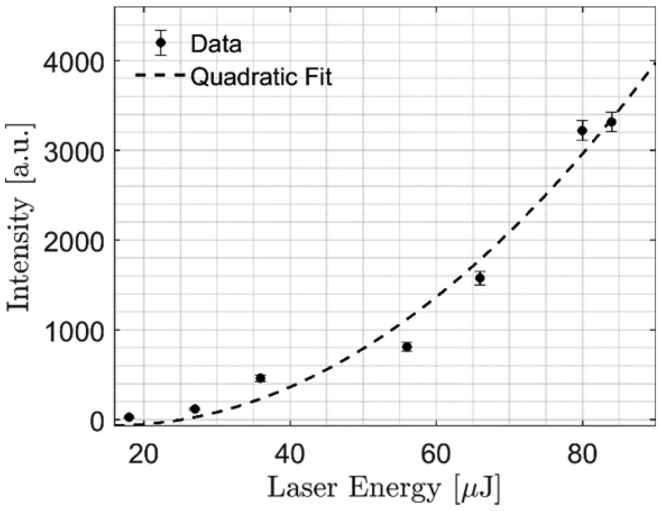

Figure 3. STARFLEET signal intensity as a function of laser energy. Energy shown indicates laser energy at the exit of the FHG, energy in the test section was 32.5% these values.

to determine the wavelength corresponding to peak resonance (λ_{peak}). This is demonstrated in figure 2, where data points are represented by dots, a Gaussian fit to the data is shown as a solid line, and the peak of the fit is shown as an open diamond. This method of determining peak excitation-pulse wavelength is the same as that used by Jiang *et al* to determine that a nearly seven-fold enhancement of fluorescence signal could be obtained by resonant excitation of nitrogen [31]. In the present work, λ_{peak} was determined to be approximately 0.5 nm lower than the peak wavelength found by Jiang *et al* and used in previous applications of the STARFLEET technique [31, 33, 34]. As a result of this wavelength study, a center wavelength of 201.75 nm was chosen for the experimental campaign described in this report.

3.2. Energy study

In addition to selecting the optimal resonance excitation-pulse wavelength, a study on the effect of laser energy was conducted to better understand the scaling of the signal intensity and ensure peak STARFLEET signal intensity was utilized in further testing. A similar study was carried out by DeLuca *et al* for the FLEET technique and found the maximum signal intensity scales linearly with laser energy, but investigated a pulse energy range on the order of mJ/pulse, rather than the μJ/pulse used in the current studies [25]. Research conducted by Pouya *et al* showed that frequency-doubled resonant femtosecond MTV signal intensity (as a function of power) was best approximated by a quadratic function [39]. In the current work, laser energy was varied from 18 μJ/pulse to 84 μJ/pulse and the STARFLEET signal intensity was recorded by the imaging system. Peak signal intensity recorded by the camera was averaged for 400 images to account for minor fluctuations in the laser power. Results of the energy study are summarized in figure 3, where data points are shown as dots, with error bars representing the uncertainty in the mean, and a quadratic fit to the data is shown as a dashed line. The energy reported in this study indicates the laser energy at the exit of the FHG, and is illustrative of how much potential signal was forfeit due to optical transmission losses. While figure 3 indicates that the intensity approximately follows a quadratic, previous studies have shown the STARFLEET signal to be linear with energy after passing a certain threshold [31]. This discrepancy, which is likely the results of using less than 5% of the laser intensity as the seminal work, has other implications that will be shown in the following subsection. Regardless of the study conducted, all results indicate that a larger laser pulse energy corresponds to higher STARFLEET signal intensities over the range of pulse energies investigated. As a result, the maximum output laser energy of approximately 90 μJ/pulse was used for the results obtained in the present work.

3.3. Spectral study

The final fundamental STARFLEET study conducted prior to the experimental campaign involved an investigation of the STARFLEET signal spectrum. The spectrum of the STARFLEET signal in a 300 K nitrogen jet flow was measured using an Ocean Optics model USB4000 spectrometer, and calibrated against the known lines of a mercury-argon light source. A total of five spectra, each consisting of a 20 s integration time, were averaged together before subtracting an averaged background spectrum. The background-subtracted spectrum is shown in figure 4(a). This spectrum shows strong signal in the UV attributable to the N_2 second positive and first negative bands (~300–440 nm), but shows very little signal in the visible range attributable to the N_2 first positive band (~500–900 nm), which is associated with the FLEET signal used for velocimetry [36]. This also differs from results reported by Jiang *et al*, which indicated a majority of the STARFLEET

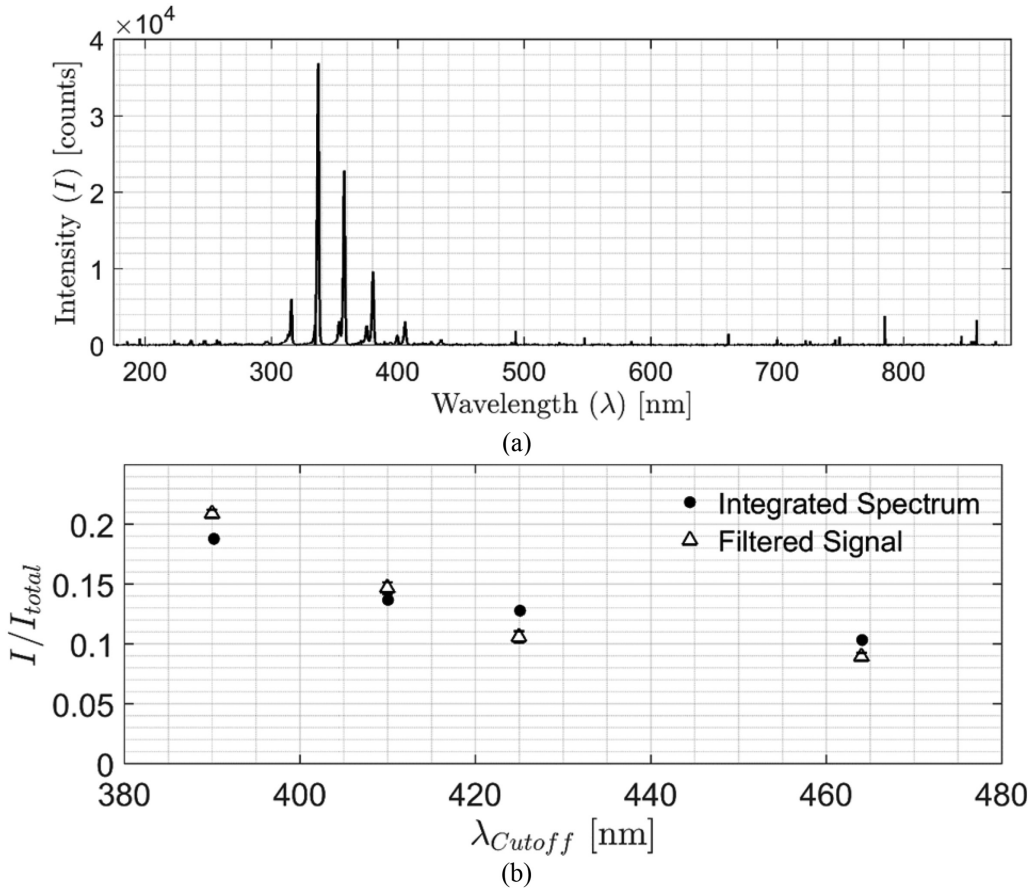

Figure 4. STARFLEET emission spectral behavior. (a) Spectrum of the STARFLEET signal as measured by a spectrometer. (b) Relative signal intensity as a function of filter cutoff wavelength, comparing the integrated spectrometer spectrum to the delayed signal detected by the camera using Wratten long-pass filters at various cutoff wavelengths. Both methods indicate that a majority of the emission is in the UV.

signal occurring at wavelengths longer than 550 nm [31], though a spectrum extending above 359 nm was never shown. With the lower laser intensity and higher gas molecule number density used in the present work (compared with [31]), the STARFLEET excitation and emission mechanism could be significantly different. In the current experiment, multi-photon absorption induced emission and dissociation might dominate; however, in the low number density conditions used by Jiang *et al*, STARFLEET might be dominated by multi-photon absorption induced ionization and dissociation. A more detailed study may be warranted to further explain these different excitation pathways, but lies outside the scope of this paper, as the focus of this work is the application of the STARFLEET technique.

To confirm the results obtained using the spectrometer, delayed STARFLEET emission was also imaged through a series of Wratten long-pass filters. By first taking unfiltered images of the STARFLEET signal and averaging them together, a total intensity could be determined for the emission resulting from resonant excitation of nitrogen. After obtaining a measurement for total intensity seen by the imaging system, a $\lambda_{\text{cutoff}} = 464$ nm long pass filter was placed in front of the objective lens and another series of images were taken and averaged together. This averaged, filtered signal was then divided by the total signal to give a relative intensity coming from the spectral region at wavelengths higher than 464 nm. This process was repeated with three additional filters at $\lambda_{\text{cutoff}} = 425$ nm, 410 nm, and 390 nm; results are summarized as open triangles in figure 4(b). These results are compared against the results obtained using the spectrometer by summing all signal from λ_{cutoff} to the end of the measured spectrum, then diving by the sum of the entire spectrum. A comparison of the integrated spectrum and filtered signal results is given in figure 4(b), where dots represent the integrated spectrum, and open triangles show the STARFLEET signal with error bars representing uncertainty in the mean. Unfortunately, the authors did not have access to Wratten filters with a λ_{cutoff} below 390 nm; however, the value and trend of the filtered results agrees well with those obtained by integrating the measured STARFLEET spectrum. Residual differences in the two techniques can be attributed to the 'soft cutoff' edge of the Wratten filters and the fact that measurements were taken at different times. As a result of this spectral study, a UV-sensitive spectrometer (LaVision HS-IRO) with an S20 photocathode was used to image the STARFLEET signal. This imaging system is similar to the UV-sensitive intensifiers and cameras used in previous STARFLEET studies [31, 33, 34].

4. Data processing

This section will describe each processing step used to transform raw data into final velocity and signal lifetime results. Subsection 4.1 describes the preprocessing applied to raw data, including background subtraction, scaling, signal binning, and image dewarping to remove lens and perspective distortion. The determination of peak STARFLEET signal and the corresponding location of maximum intensity is covered in subsection 4.2. Finally, the methods used to determine flow velocity and signal lifetimes are discussed in subsection 4.3.

4.1. Preprocessing

The first step in processing raw STARFLEET data is subtracting the background signal and applying an image dewarping to correct each frame for lens effects and perspective distortion resulting from the oblique camera viewing angle. Prior to the experiment, a set of calibration images were taken of a target placed parallel to the path of the laser in the imaging plane. The target consisted of a regular grid pattern of small dots with 6.2 mm spacing between each point. The location of each dot is determined in the calibration images using a custom centroid-finding algorithm, and all points are then mapped to their respective expected location given the known target pattern. With the image transformation determined in this way, the same transformation could then be applied to all frames containing STARFLEET data. Additionally, since the physical spacing between the target dots is known, this dewarping method also allows for the extraction of a scale factor that is used to convert pixel spacing into physical units. A typical time series showing all 10 frames of single-shot, background-subtracted, and dewarped images is given in figure 5(a), while an averaged series (of 1000 shots per image) is shown in figure 5(b). For each image in figure 5, the dark vertical line is the STARFLEET signal which advects from left to right with the flow, allowing for the extraction of velocity and acceleration. In addition to tracking rightward in each subsequent frame, the signal is also seen to diminish in time; this signal decay will allow for the extraction of a signal lifetime, as discussed in subsection 4.3.

The final step in data preprocessing involved binning the data into a single bin in order to better compare with the signal obtained in previous experiments. While the spatially-distributed STARFLEET signal obtained in the present study can provide important flow information (such as single-shot velocity profiles [33, 34]), these benefits do not outweigh the disadvantages associated with this method of imaging (e.g. reduced signal-to-noise ratio) given the steady, freestream flow considered in this experimental campaign. Resultantly, and at the cost of reduced spatial resolution, the extended STARFLEET emission data was binned into a single bin to increase the signal-to-noise ratio (SNR) and more closely resemble previous results obtained using the boresight (or quasi-boresight) configuration [28, 30, 36–38] which served to integrate all signal onto a single region of the detector. After binning each frame of data, STARFLEET

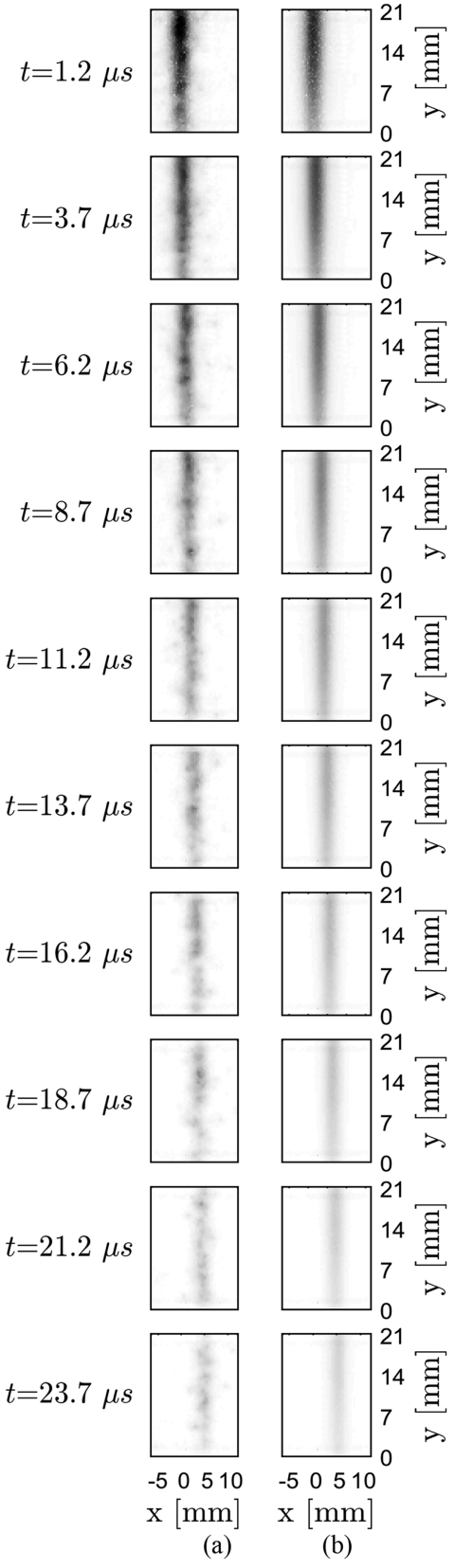

Figure 5. Time series of background-subtracted, dewarped STARFLEET data for $M = 0.5$, $P = 276$ kPa, $T = 150$ K case. (a) Representative single-shot dataset. (b) Time-averaged signal. STARFLEET emission is the dark vertical band, and flow is left-to-right.

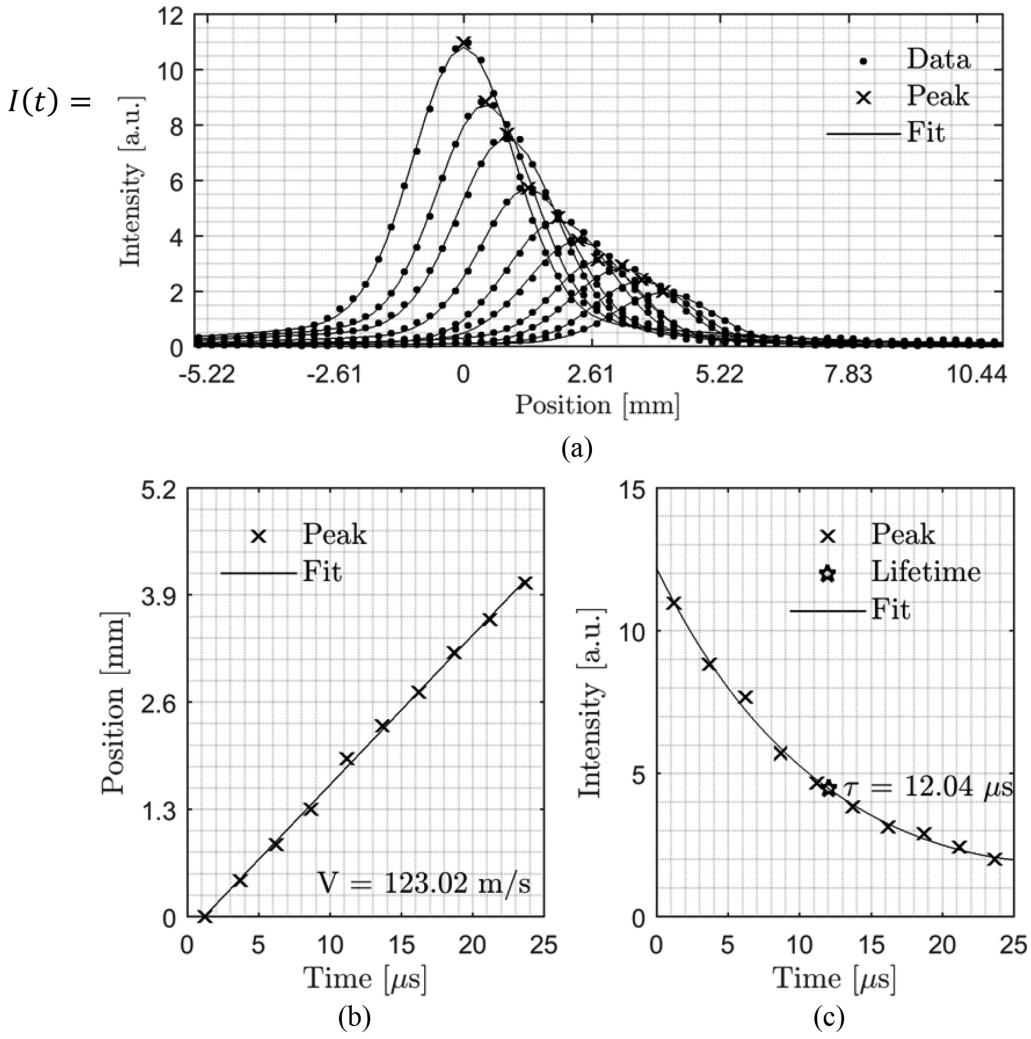

Figure 6. STARFLEET signal peak intensity, position, velocity and lifetime measurements. (a) Intensity profiles for all 10 frames of signal are shown as solid lines. Profiles are fit to experimental data (marked by '·') with '×' indicating the location and value of peak intensity for each frame. (b) Peak signal position as a function of time and corresponding fit for velocity (based on the slope of the line). (c) Peak intensity as a function of time and corresponding fit, with a star indicating the measured STARFLEET signal lifetime.

profiles were obtained and used to quantify the maximum signal, as well as determine the corresponding location of peak-intensity to sub-pixel accuracy. Typical profiles are shown as dots in figure 6(a) and discussed further in the following subsection.

4.2. Peak-signal determination

With the STARFLEET signal profiles determined as described in the previous subsection, those results can be used to find the value and position of the peak signal. This is done by fitting a Gaussian model to the preprocessed STARFLEET data in order to determine the peak signal location with sub-pixel accuracy:

$$G(x) = c_0 + a_1 \exp\left[-\left(\frac{x - b_1}{c_1}\right)^2\right], \tag{1}$$

where the first term is fit to the background signal, ensuring that the second term of $G(x)$ provides a proper fit to the STARFLEET signal. The Gaussian model is shown fit to data as the solid lines in figure 6(a). From this Gaussian model fit, the peak value is used to determine the maximum STARFLEET signal for each frame, and the location corresponding to peak intensity can be determined to sub-pixel accuracy. This peak intensity and location is marked by '×' for each of the 10 frames of data in figure 6(a) for the $M = 0.5$, $P = 276$ kPa, $T = 150$ K case. As expected, the peak signal moves rightward with the flow in each subsequent frame, and also shows signal decay in time:

$$I(t) = ae^{bt} + ce^{dt}. \tag{2}$$

4.3. Velocity and signal lifetime calculations

Since more than two frames of STARFLEET signal were captured in the present work, there are several ways to extract velocity from the peak signal locations determined as described in the previous subsection. Studies by Burns *et al* have shown that the highest measure of accuracy and precision

could be obtained using the linear regression method [36, 38], and so a similar linear fitting method (with several constraints introduced to ensure only valid and physical velocity results were considered) was chosen to perform velocity calculations in this paper. To ensure frames with low SNR are rejected from consideration, intensity thresholding was used to only include data with STARFLEET signal intensities above a set value. This restriction eliminated about 3% of the frames. For all peaks passing this criteria, the corresponding location was plotted against time, as shown marked by '×' in figure 6(b). Once the peak signal location for all frames in a given set were plotted against time, a line was fit to all data points that passed the intensity thresholding; this is shown by a solid line in figure 6(b). To further ensure only valid velocity results we considered, all velocity fits with $R^2 < 0.97$ were excluded from further analysis; typically this constraint eliminated less than 5% of the fits for each condition. The flow velocity is then determined by the slope of the fit line. This analysis method is appropriate for the measurement of freestream flow, as considered in this work, since acceleration and steep gradients are expected to be negligible.

In addition to extracting velocity measurements, the peak signal determination described in the previous subsection can also be used to calculate the STARFLEET signal lifetime. Rather than plotting the position as a function of time, if instead the peak signal intensity is plot in time, then a bi-exponential curve can be fit to the data, STARFLEET peak intensities are shown plotted against time as '×' in figure 6(c), while the bi-exponential fit to data is shown as a solid line. The signal lifetime can then be defined to be the time that the signal reaches $1/e$ of the original value, and is shown as a star in figure 6(c).

5. Results and discussion

This section will cover results obtained from 45 different run conditions spanning the entire test envelope of the 0.3 m TCT. Thermodynamic dependences of the STARFLEET signal intensity and lifetime are explored in subsection 5.1, while general observations about the freestream velocity measurements (and the ability of the facility to reach and maintain 'on-point' conditions) are discussed in subsection 5.2. The accuracy and precision of velocity results are reported in subsections 5.3 and 5.4, respectively. A discussion regarding the data obtained, and more generally STARFLEET as a viable measurement technique for use in large-scale, cryogenic wind tunnels, is offered in subsection 5.5.

5.1. Thermodynamic dependences of STARFLEET signal intensity and lifetime

Signal intensity and lifetime measurements captured at each run condition provide insight into the behavior of the STARFLEET technique and its potential for successful application in TCTs. The average lifetimes and initial signal intensities are plotted as a function of various thermodynamic conditions in figure 7, where 1000 shots were used to compute the statistics at each point and error bars show one standard deviation uncertainty. Signal intensity data, shown along the top row of figure 7, were collected approximately 1.2 μs after the laser pulse. Figures 7(a) and (b) show that flow pressure and temperature have little effect on the spread and uncertainty of signal intensity measurements; however, a general reduction in peak STARFLEET signal intensity is observed with increasing pressure and decreasing temperature. These combined pressure and temperature effects suggest a strong density dependence, and figure 7(c) confirms an inverse linear dependence on flow density. This trend becomes even more evident when considering independently the effect of pressure and temperature. The maximum STARFLEET signal intensities observed in these studies occur at the highest temperature and lowest pressure, corresponding to the lowest density considered. If temperature is maintained while pressure is increased, density is increased and the signal intensity drops accordingly, as indicated by the red symbols in figure 7(c). Similarly, if pressure is maintained while temperature is dropped, density increases and the STARFLEET signal intensity is further reduced, as indicated by the colored triangular symbols in figure 7(c). Despite the clarity of the inverse relation between density and STARFLEET signal, this trend is opposite that found for the FLEET technique, where signal was shown to scale linearly with density [28]. Additionally, Burns *et al* observed that FLEET displayed 'very poorly defined thermodynamic dependences with respect to signal intensity' at the delay times considered in this study [28]. In contrast, STARFLEET signal intensity results show a strong dependence on the thermodynamic state of the flow regardless of the considerable delay used in the current work (though reduced scatter and a stronger dependence is expected for shorter delay times).

As with intensity, signal lifetime measurements are plotted against pressure, temperature, and density, and results are shown along the bottom row of figure 7. Unlike signal intensity data, lifetime measurement spread and uncertainty show a strong dependence on both pressure and temperature. As shown in figures 7(d) and (e), larger spread and uncertainty are seen for higher pressures and lower temperatures, respectively. Another way to view this same phenomenon is that the STARFLEET lifetime is less sensitive to pressure at higher temperatures, but shows a much stronger dependence on pressure as temperature is lowered. Again, once the data is plotted against density, as shown in figure 7(f), the reason for this trend becomes evident; STARFLEET signal lifetime scales proportionally with density. Figure 7(f) clearly shows that both the signal lifetime and the uncertainty increase with increasing density, with one important exception. The only runs that do not appear to agree well with this trend are the highest pressure, lowest temperature cases, indicated by the dark blue triangular symbols. An explanation for this inconsistent behavior is presented and discussed further in subsection 5.4. Finally, the general trends observed in lifetime measurements as a function of pressure, temperature, and density demonstrate an inverse behavior to the thermodynamic dependences displayed by the corresponding signal intensity measurements, as well as behavior opposite that of the lifetime results measured using the FLEET technique [28].

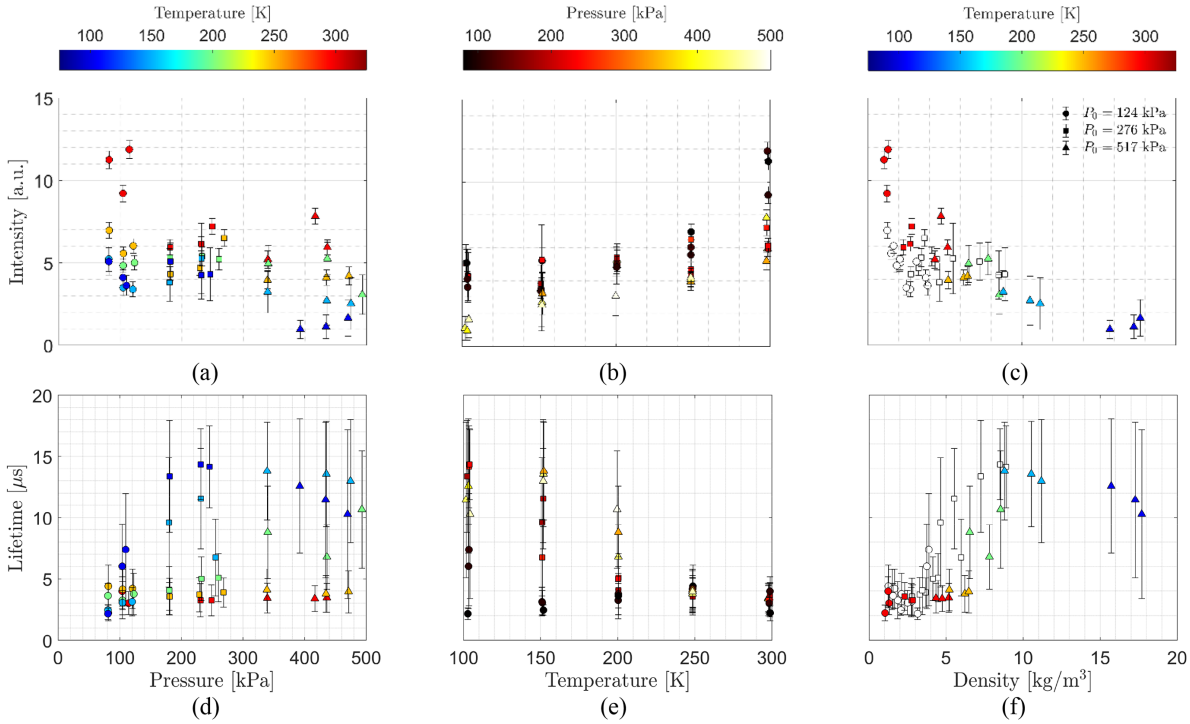

Figure 7. Signal intensity at 1 µs and lifetime measurements as a function of thermodynamic conditions for all 45 run conditions. Intensity as a function of (a) pressure, (b) temperature, and (c) density. Lifetime as a function of (d) pressure, (e) temperature, and (f) density.

5.2. *Freestream velocity measurements*

Much in the same way that signal intensities and lifetimes were averaged to yield a single value for each of the 45 run conditions considered in this experimental campaign, all valid single-shot velocity measurements were averaged to provide a mean velocity at every freestream flow condition. Velocity measured using the STARFLEET technique is plotted as a function of temperature, pressure, and Mach number in figure 8; symbols indicate velocity measurements at various pressures, while line type represents the nominal $M = 0.2$, $M = 0.5$, and $M = 0.8$ velocities predicted by isentropic flow theory. The apparent discrepancy between certain measured velocities and the values predicted by isentropic flow theory was not a limitation of the technique itself, but rather with the 0.3 m facility, which was unable to achieve the nominal Mach conditions. The difference between the nominal condition and the velocity achieved by the 0.3 m facility is indicated by the symbol color of each velocity measurement. In addition to the inability of the 0.3 m TCT to maintain set point for some conditions, some slight-but-noticeable spread in velocity is attributable to variability in the set-point conditions within the wind tunnel facility. In other words, a majority of the observable deviation is not necessarily experimental scatter, but rather due to the fact that the true Mach number may vary from the normal condition by as much as two percent due to limitations in the tunnel drive system [36]. Figure 8 demonstrates that not only is STARFLEET sufficiently sensitive to resolve the expected physical trend of increasing velocity with increasing temperature for the range considered in this study, but was also sensitive enough to detect when the facility was not at

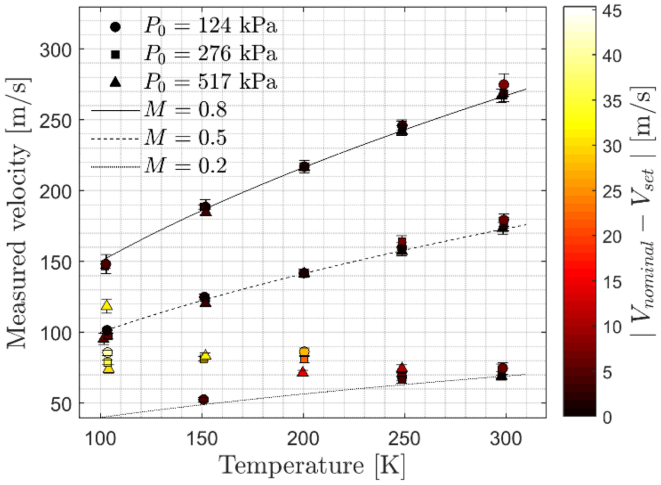

Figure 8. Measured velocity as a function of temperature shows that the STARFLEET technique is sufficiently sensitive to measure the expected increase in velocity with increasing temperature.

the nominal Mach number. Evidence that the STARFLEET technique provides the expected velocity (regardless of the facility's ability to maintain each condition) is provided in the following subsection, as is a more detailed discussion regarding the accuracy of STARFLEET velocity measurements.

5.3. *Velocity measurement accuracy*

STARFLEET velocity measurement accuracy in the 0.3 m TCT was assessed through comparison with values obtained

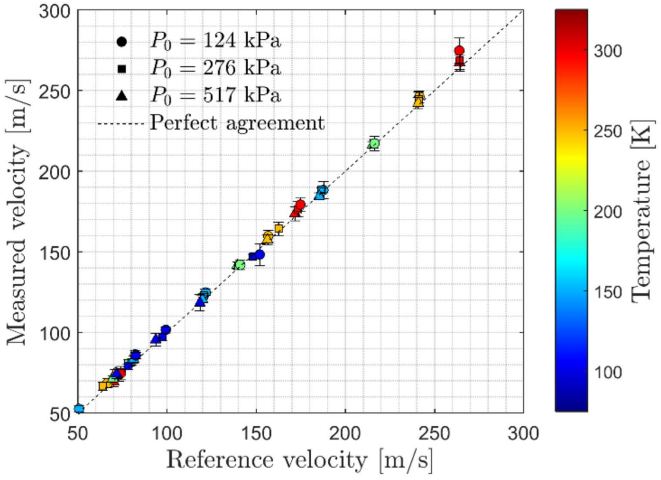

Figure 9. Measured velocity as a function of the 0.3 m DAS reference velocity and temperature, where the dashed line represents perfect agreement. Accuracy is generally independent of thermodynamic conditions.

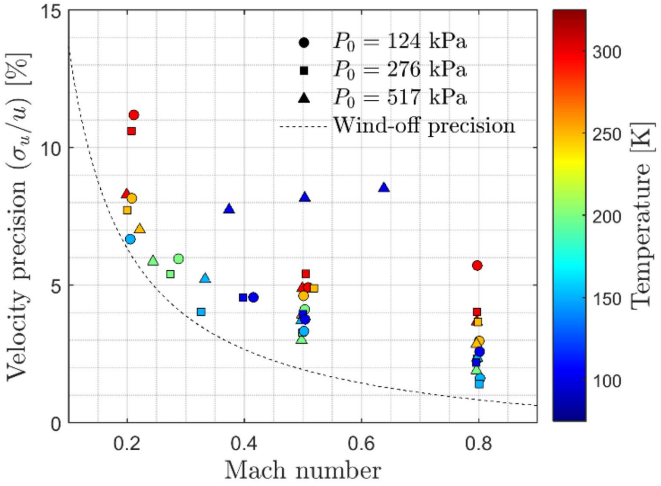

Figure 10. Velocity precision (as a percentage of flow velocity) as a function of Mach number and temperature, where the dashed line represents the wind-off precision across all Mach numbers. An overall improvement in precision (reduction in percentage) is seen with increasing Mach number, while higher temperatures generally correspond to worse precision (larger percentage of freestream velocity).

by the facility DAS. Measured velocity for all 45 conditions considered in this study are shown plotted against the DAS reference velocity in figure 9, where the colored symbols indicate freestream flow velocity measurements and the dashed line represents perfect agreement between the facility DAS and the STARFLEET estimates. Qualitatively, the STARFLEET velocity measurements align well with those acquired by the facility, regardless of pressure or temperature. As observed in previous MTV experiments in the 0.3 m TCT [28, 33, 34], a slight discrepancy between the two methods of measuring velocity appears to grow larger with increasing velocity. While this discrepancy could be partly caused by a number of errors (including calibration error, the dewarping algorithm failing to sufficiently remove perspective distortion, or inherent error associated with single-line tagging methods [40, 41]), previous studies have shown that this discrepancy can be remedied by applying an additional correction factor to account for the diverging walls of the test facility [30]. The aggregate accuracy of the measurements is presented quantitatively using the standard error (ε), defined as

$$\varepsilon = \frac{\sum_{i=1}^{n} |v_i - v_{i,DAS}|}{\sum_{i=1}^{n} |v_{i,DAS}|}. \tag{3}$$

When presented as a percentage, the standard error represents the average percent error of all velocity measurements included in the calculation. Standard error was found to be 1.6%, which is consistent with previous FLEET and PLEET measurements in the 0.3 m TCT that found the accuracy to lie between 0.6% and 2.1% [28, 30, 42]. This standard error also shows that the STARFLEET method not only performs roughly as well as laser Doppler velocimetry in the 0.3 m TCT (which obtained typical velocity measurement error less than 1% [22]), but does so more consistently and over a broader range of conditions. STARFLEET also compares favorably with other velocimetry techniques, including air photolysis and recombination tracking (APART) [43], acetone MTV [44], and hydroxyl MTV [45], which have demonstrated accuracies within 5%, 3.2%, and 2%, respectively, though not in transonic cryogenic wind tunnels. In summary, the STARFLEET technique is shown to provide similar accuracies to a number of other velocimetry methods, but without the need to seed the flow, use multiple lasers, or cause large thermal perturbations within the measurement region.

5.4. Velocity measurement precision

Precision at each flow condition (σ_u) was taken to be the standard deviation of all valid single-shot velocity measurements within a given set. Note that measurement precision can be affected by bin size owing to spatial averaging. STARFLEET precision measurements (normalized by the freestream flow velocity) are shown as a function of Mach number in figure 10, where symbol type indicates pressure, color shows temperature, and the dashed line is the wind-off precision as defined by Burns *et al* [28]. Generally, percent precision is shown to improve (decrease in σ_u/u) with an increase in Mach number and a reduction of temperature. The improvement with Mach number is mainly owing to dividing by a larger velocity, whereas the improvement at lower temperatures is caused by the increased signal lifetime resulting from higher densities. Some obvious exceptions to this trend are the three highest pressure, coldest conditions considered (indicated by the dark blue triangles). The reason for these three exceptions, as well as the lower-than-expected signal lifetime measurements at these same conditions (as shown in figure 7(f) and discussed in subsection 5.1), are attributable to two main factors. The first factor is that defining the precision to be the standard deviation of velocity measurements does not distinguish between precision errors in the velocity measurements and natural turbulent fluctuations. Since the magnitude of the freestream velocity fluctuations depends on Reynolds number, which increases both with decreasing temperature

and higher pressure, some loss of precision is expected at these high Reynolds number conditions owing to turbulence. Part I of this series of papers describing FLEET velocimetry also demonstrated reduced precision with increasing Reynolds number. These FLEET measurements additionally serve to establish an upper bound on the stability of freestream velocity fluctuations in this facility [28]. These previous studies indicate that the velocity fluctuations in the 0.3 m TCT freestream are typically 0.5% of the mean velocity. Thus, real freestream velocity fluctuations do not contribute significantly to the overall precision assessment of the STARFLEET technique since the observed fluctuations are significantly higher than the actual velocity fluctuations. The second reason for the diminished precision of the highest-density cases is a result of the STARFLEET technique responding to the thermodynamic conditions of the flow, as well as the poor operation of the facility at these conditions. Given the dependence of σ_u/u on flow temperature and the fact that density is proportional to signal lifetime, the three highest-density run conditions should be some of the most precise cases; however, at roughly 8% of the freestream velocity (regardless of Mach number), they are among the least precise of all conditions considered in this study. The precision does not continue to improve as temperature is dropped and pressure is increased because the flow conditions are approaching the liquid-vapor saturation point of nitrogen. As conditions near the saturation point, liquid nitrogen droplets no longer evaporate and begin to interfere with the laser focusing and formation of the STARFLEET signal. This accounts for the shorter lifetimes and reduced signal intensity, in turn causing a reduction in velocity measurement precision. Figure 11 shows the total velocity precision (σ_u in m s^{-1}) for all 45 run conditions as a function of pressure and temperature, with the liquid-vapor saturation point as a dashed line. Velocity precision generally improves from the lower right to the upper left (as pressure is increased and temperature is reduced); however, as conditions reach the liquid-vapor saturation point of nitrogen there is a sudden reduction in total velocity precision (increase in σ_u). This trend also correlates well with signal lifetime measurements, where lifetime is observed to increase with density until a sudden reduction is seen for the highest density cases, providing further evidence that nearing the saturation point is detrimental to both signal lifetime and STARFLEET velocity measurement precision. While FLEET measurements also demonstrated a reduced precision as the saturation point was approached, the FLEET technique displayed an opposite thermodynamic dependence to STARFLEET, with an overall improvement in total velocity precision as pressure was reduced and temperature was increased [28]. Regardless of the uncharacteristically imprecise highest-density runs, precision measurements show the STARFLEET technique to be roughly an order of magnitude worse than previous FLEET results [28] and approximately a factor of two worse than PLEET precision measurements [30].

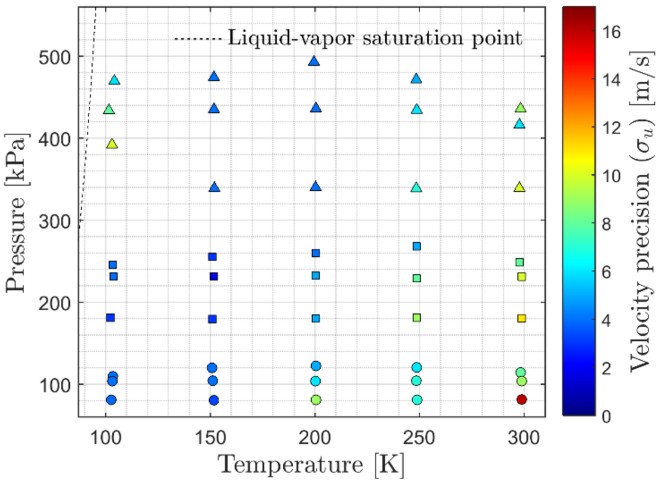

Figure 11. Total velocity precision as a function of pressure and temperature.

5.5. Discussion

The results presented in this section have provided valuable insight into the utility of STARFLEET as a viable diagnostic technique for application in TCTs. Investigation of the signal intensity and lifetime has shown a strong dependence on the thermodynamic conditions of the flow, especially considering the data was taken after a considerable delay from initial signal generation compared with delays used in previous studies [28]. In this work, a delay of 1 µs was used to avoid the rapid loss of signal in early frames due to the double exponential decay of intensity, allowing for a more balanced signal between early frames and later frames. Investigation of the maximum STARFLEET signal showed intensity to be inversely proportional to density, while lifetime measurements demonstrated nearly linear scaling with density until conditions approached the liquid-vapor saturation point. Longer lifetimes were also shown to correlate with higher precision measurements of velocity, while accuracy showed little dependence on thermodynamic conditions. Standard error measurements prove that the STARFLEET technique provides similar (or better) accuracy to other velocimetry methods, but does not require seeding of the test gas nor does the method significantly thermally perturb the measurement region, as with alternative methods. While accuracy is similar to other MTV techniques, precision is shown to be worse than measurements made using FLEET or PLEET; however, the relative imprecision of measurements seen in this study are partially a result of reduced SNR, due to low reflectivity (~85% at each mirror) for the deep-UV, ultrafast laser pulses. Mirrors prohibiting high-reflectivity and the expensive MgF_2 optics for windows and lenses required to transmit and focus the beam are two of the major shortcomings of STARFLEET which need to be addressed when considering application of this technique. Because a cold, high-pressure, high-density environment is favorable for the technique, STARFLEET is a promising viable candidate for velocimetry in TCTs. The method used to determine flow velocity will depend on several factors, all of which should be considered before choosing a diagnostic technique. If high precision measurements are required, one might consider instead using FLEET, as this method provides the most precise velocity measurements

Table 1. Comparison of FLEET, PLEET and STARFLEET setup and performance parameters.

Criteria	FLEET	PLEET	STARFLEET
Laser pulse duration	70 fs	100 ps	>92 fs[a] [46]
Laser repetition rate	1 kHz	10–100 kHz	1 kHz
Excitation wavelength	800 nm	1064 nm	201.8 nm
Typical energy used per pulse	0.5–2 mJ	10–40 mJ	25–90 μJ
Temperature perturbation from energy deposition at STP using energy to generate comparable signal intensity [31]	230 K with 1.1 mJ	250 K with 10 mJ	10 K with 30 μJ
Average measurement accuracy (error) in 0.3 TCT	~1% of measured velocity	~1% of measured velocity	~1% of measured velocity
Zero-velocity measurement precision (1σ) in 0.3 m TCT	0.4 m s^{-1}	1.2–2 m s^{-1}	2.8 m s^{-1}
Suitable test media (demonstrated)	Freon [47], combustion [48], nitrogen, air	Nitrogen	Nitrogen, air
Thermodynamic dependence of signal intensity for typical TCT conditions ($100 < T < 300$ K, $100 < P < 517$ kPa)	Intensity ~ρ	None	Intensity ~1/ρ
Thermodynamic dependence of signal lifetime for typical TCT conditions ($100 < T < 300$ K, $100 < P < 517$ kPa)	Lifetime ~1/ρ	Lifetime ~1/P	Lifetime ~ρ

[a]Fourth-harmonic generation of the 201.8 nm beam increases the laser pulse duration; however, the exact pulse duration was not directly measured in this work. See reference for more information.

and does not require the use of a fourth-harmonic generator. Should time-resolved velocity be desired, the PLEET method would be better applied, as this method allows for high-repetition-rate measurements. If surface damage or thermometry within the measurement region need to be considered, STARFLEET is likely the best candidate due to the resonant (and thus less thermally-perturbative) nature of the technique. A summary comparing several important performance parameters (e.g. excitation wavelength, energy/pulse, and laser repetition rate) for the above three techniques is provided in table 1.

Finally, it is important to note that while a majority of the preliminary studies described in section 1 agreed well with earlier fundamental STARFLEET results (e.g. resonance excitation at 202 ± 0.25 nm and signal intensity dependence on laser energy), the spectrum of the STARFLEET signal was different from that reported by Jiang *et al* [31]. Based on the work of Jiang, the signal associated with the first positive band of nitrogen should be dominant [31]; however, neither the spectrometer measurements nor the filtered images of the delayed STARFLEET emission shown in the present studies indicated this to be the case. One possible explanation for this discrepancy is that the lower laser energy and slower optics used to focus the beam led to less than 1/20th of the laser intensity being used to write the STARFLEET line compared with that used by Jiang *et al* These substantial intensity differences could potentially have a significant effect on the STARFLEET signal and N_2 recombination mechanism (for example causing higher C-B emission relative to B-A), leading to the dominant signal coming from the UV in the current work. Further investigation into these differences may be warranted, but lies outside the scope of this paper.

6. Conclusions

STARFLEET velocimetry has been characterized and investigated for use in TCTs. Initial fundamental studies showed peak resonance at 201.75 nm, increasing signal intensity with increasing laser energy, and strong emission in the UV. Following this preliminary testing, which helped to guide the experimental setup, STARFLEET velocimetry was applied in the NASA Langley 0.3 m TCT to obtain measurements across the entire operational envelope of the facility. Raw data was processed to allow for the extraction of signal lifetime and velocity measurements. Maximum STARFLEET signal intensity was shown to be inversely proportional to density, while lifetime was nearly linear with density until approaching the liquid-vapor saturation point of nitrogen. Velocity measurements were assessed for accuracy, and showed a standard error of 1.6%, which is comparable to other unseeded, laser-based MTV techniques (which generally provided accuracy in the range of 0.6%–2.1%). Accuracy was also shown to be independent of the thermodynamic state of the flow. STARFLEET precision was also investigated, and showed precision from approximately 1.5%–10% of the freestream velocity. Percent precision was shown to generally improve with increasing Mach number and a reduction of temperature, until reaching the saturation point. The precision of STARFLEET is generally an order of magnitude worse than the FLEET technique, and roughly a factor of two worse than PLEET; however, this relatively poor precision is partially due to low SNR resulting from energy losses at each turning mirror and could be improved if better or fewer mirrors were used.

While the STARFLEET technique ultimately allowed for unseeded, non-intrusive velocity measurements in a cryogenic environment, there are several factors that need to be

considered prior to applying this technique in a TCT. First, oxygen absorption and the inability of mirrors to provide high reflectivity (>95%) of the ultra-fast UV laser beam leads to a significant reduction of energy reaching the measurement volume. Additionally, expensive MgF_2 windows and focusing optics must be used to transmit the deep UV laser beam. If more precise measurements are required and large thermal perturbations and surface damage are not a concern, the FLEET technique is likely a better option. Similarly, PLEET would be better applied if high-repetition-rate measurements are required. However, if energy losses can be tolerated and surface damage or thermometry must be considered, the STARFLEET technique is a suitable candidate for providing velocimetry measurements in a large-scale, high-pressure, cryogenic wind tunnel.

Acknowledgements

The authors would like to thank the entire staff at the 0.3 m TCT for their assistance during testing, as well as Sukesh Roy of Spectral Energies, LLC for his support during this project. The authors also wish to thank Ross Burns for his invaluable input to this paper. Funding for this research was provided by a NASA Langley Research Center Internal Research and Development (IRAD) Project and NASA's Aerosciences Evaluation and Test Capabilities (AETC) Portfolio, as well as NASA's Small Business Innovation Research (SBIR) NNX14CL74P and NNX15CL24C, and the U.S. Air Force Office of Scientific Research (AFOSR) award numbers 15RQCOR202 and 14RQ06COR.

ORCID iDs

Daniel T Reese https://orcid.org/0000-0002-0294-2814
Paul Danehy https://orcid.org/0000-0001-9795-7754

References

[1] Fuller Dennis E, Gloss B B and Nystro D 1981 Guide for users of the national transonic facility *NASA Technical Memorandum* 83124
[2] Ladson C L and Ray E J 1987 Evolution, calibration, and operational characteristics of the two-dimensional test section of the Langley 0.3 meter transonic cryogenic tunnel *NASA TP-2749*
[3] Snow W L, Burner A W and Goad W K 1982 Image degradation in Langley 0.3 meter transonic cryogenic tunnel *NASA Technical Memorandum* 84550
[4] Snow W L, Burner A W and Goad W K 1987 Improvement in the quality of flow visualization in the Langley 0.3 m transonic cryogenic tunnel *NASA Technical Memorandum* 87730
[5] Burner A W, Goad W K, Massey E A, Goad L R, Goodliff S L and Bissett O W 2008 Wing deformation measurements of the DLR-F6 transport configuration in the national transonic facility AIAA 2008–6921
[6] Burner A W, Wahls R A and Goad W K 1996 Wing twist measurements at the national transonic facility *NASA Technical Memorandum* 110229
[7] Pallek D, Bütefisch K A, Quest J and Strudthoff W 2003 Model deformation measurement in ETW using the Moire technique *20th Int. Congress on Instrumentation in Aerospace Simulation Facilities* (*Goettingen, Germany*)
[8] Fey U, Engler R H, Egami Y, Iijima Y, Asai K, Jansen U and Quest J 2003 Transition detection by temperature sensitive paint at cryogenic temperatures in the european transonic windtunnel (ETW) *20th Int. Congress on Instrumentation in Aerospace Simulatin Facilities* (*Goettingen, Germany*)
[9] Fey U, Konrath R, Kirmse T, Ahlefeldt T, Kompenhans J and Egami Y 2010 Advanced measurement techniques for high Reynolds number testing in cryogenic wind tunnels *48th AIAA Aerospace Sciences Meeting Including the New Horizons Forum and Aerospace Exposition* (*Orlando, FL*) AIAA-2010-1301 pp 1–8
[10] Watkins A N, Leighty B D, Lipford W E, Oglesby D M, Goodman K Z, Goad W K, Goad L R and Massey E A 2009 The development and implementation of a cryogenic pressure sensitive paint system in the national transonic facility *47th AIAA Aerospace Sciences Meeting Including the New Horizons Forum and Aerospace Exposition* (*Orlando, FL*) AIAA-2009-421 pp 1–10
[11] Watkins A N *et al* 2005 Flow visualization at cryogenic conditions using a modified pressure sensitive paint approach *43rd AIAA Aerospace Sciences Meeting and Exhibit* (*Reno, NV*) (https://doi.org/10.2514/6.2005-456)
[12] Yorita D, Klein C, Henne U, Ondrus V, Beifuss U, Hensch A K, Guntermann P and Quest J 2016 Application of lifetime-based pressure-sensitive paint technique to cryogenic wind tunnel tests *54th AIAA Aerospace Sciences Meeting* (*San Diego, CA*) (https://doi.org/10.2514/6.2016-0649)
[13] King R A, Andino M Y, Melton L, Eppink J and Kegerise M A 2014 Flow disturbance measurements in the national transonic facility *Aiaa J.* **52** 116–30
[14] Shirinzadeh B, Herring G C and Barros T 1999 Demonstration of imaging flow diagnostics using rayleigh scattering in Langley 0.3 m transonic cryogenic tunnel *NASA Technical Note* 1999–208970
[15] Herring G C and Shirinzadeh B 2002 Flow visualization of density in a cryogenic wind tunnel using planar Rayleigh and Raman scattering *NASA Technical Memorandum* 2002–211630
[16] Herring G C, Lee J W and Goad W K 2015 Feasibility of Rayleigh scattering flow diagnostics in the national transonic facility *NASA Technical Memorandum* 2015–218800
[17] Gartenberg E, Weinstein L M and Lee E E 1994 Aerodynamic investigation with focusing schlieren in a cryogenic wind tunnel *AIAA J.* **32** 1242–9
[18] Germain E and Quest J 2005 The development and application of optical measurement techniques for high reynolds number testing in cryogenic environment *43rd AIAA Aerospace Sciences Meeting and Exhibit* (*Reno, NV*) (https://doi.org/10.2514/6.2005-458)
[19] Quest J and Konrath R 2011 Accepting a challenge—the development of PIV for application in pressurized cryogenic wind tunnels *41st AIAA Fluid Dynamics Conf. and Exhibit* (*Honolulu, HI*) (https://doi.org/10.2514/6.2011-3726)
[20] Willert C, Stockhausen G, Beversdorff M, Klinner J, Lempereur C, Barricau P, Quest J and Jansen U 2005 Application of Doppler global velocimetry in cryogenic wind tunnels *Exp. Fluids* **39** 420–30
[21] Konrath R, Geisler R, Agocs J, Otter D, Ehlers H, Philipp F and Quest J 2015 High-speed piv applied to wake of NASA CRM model in ETW under high re-number stall conditions for sub- and transonic speeds *53rd AIAA Aerospace*

Sciences Meeting (*Kissimmee, FL*) (https://doi.org/10.2514/6.2015-1095)
[22] Gartrell L R, Gooderum P B, Hunter W W and Meyers J F 1981 Laser velocimetry technique applied to the Langley 0.3 m transonic cryogenic tunnel *NASA Technical Memorandum* 81913
[23] Honaker W C and Lawing P L 1985 Measurements in the flow field of a cylinder with a laser transit anemometer and a drag rake in the Langley 0.3 m transonic cryogenic tunnel *NASA Technical Memorandum* 86399
[24] Michael J B, Edwards M R, Dogariu A and Miles R B 2011 Femtosecond laser electronic excitation tagging for quantitative velocity imaging in air *Appl. Opt.* **50** 5158–62
[25] DeLuca N J, Miles R B, Kulatilaka W D, Jiang N and Gord J R 2014 Femtosecond laser electronic excitation tagging (FLEET) fundamental pulse energy and spectral response *30th AIAA Aerodynamic Measurement Technology and Ground Testing Conf.* (*Atlanta, GA*) (https://doi.org/10.2514/6.2014-2227)
[26] Edwards M R, Dogariu A and Miles R B 2015 Simultaneous temperature and velocity measurement in unseeded air flows with femtosecond laser tagging *AIAA J.* **53** 2280–8
[27] Limbach C M and Miles R B 2017 Rayleigh scattering measurements of heating and gas perturbations accompanying femtosecond laser tagging *Aiaa J.* **55** 112–20
[28] Burns R A, Peters C J and Danehy P M 2018 Unseeded velocimetry in nitrogen for high-pressure, cryogenic wind tunnels: part I. Femtosecond-laser tagging *Meas. Sci. Technol.* **29** 115302
[29] Jiang N, Mance J G, Slipchenko M N, Felver J J, Stauffer H U, Yi T, Danehy P M and Roy S 2017 Seedless velocimetry at 100 kHz with picosecond-laser electronic-excitation tagging *Opt. Lett.* **42** 239–42
[30] Burns R A, Danehy P M, Jiang N, Slipchenko M N, Felver J and Roy S 2018 Unseeded velocimetry in nitrogen for high pressure cryogenic wind tunnels: part II. Picosecond-laser tagging *Meas. Sci. Technol.* **29** 115203
[31] Jiang N, Halls B R, Stauffer H U, Danehy P M, Gord J M and Roy S 2016 Selective two-photon absorptive resonance femtosecond-laser electronic excitation tagging velocimetry *Opt. Lett.* **41** 2225–8
[32] Salumbides E J, Khramov A and Ubachs W 2009 High-resolution 2 + 1 REMPI study of the $a''^1\,\Sigma_g^+$ state in N_2 *J. Phys. Chem.* A **113** 2383−6
[33] Reese D, Danehy P, Jiang N, Felver J, Richardson D and Gord J 2019 Application of resonant femtosecond tagging Velocimetry in the 0.3 meter transonic cryogenic tunnel *Aiaa J.* **57** 3851–8
[34] Reese D, Danehy P, Jiang N, Felver J, Richardson D and Gord J 2018 Application of STARFLEET velocimetry in the NASA Langley 0.3 meter transonic cryogenic tunnel *AIAA Aerodynamic Measurement Technology and Ground Testing Conf.* (*Atlanta, GA*) (https://doi.org/10.2514/6.2018-2989)
[35] Kulatilaka W, Gord J, Katta V and Roy S 2012 Photolytic-interference-free, femtosecond two-photon fluorescence imaging of atomic hydrogen *Opt. Lett.* **37** 3051–3
[36] Burns R, Danehy P, Halls B and Jiang N 2015 Application of FLEET velocimetry in the NASA Langley 0.3 meter transonic cryogenic tunnel *31st AIAA Aerodynamic Measurement Technology and Ground Testing Conf.* AIAA-2015-2566 (https://doi.org/10.2514/6.2015-2566)
[37] Burns R A and Danehy P M 2017 Unseeded velocity measurements around a transonic airfoil using femtosecond-laser tagging *AIAA J.* **55** 4142–54
[38] Burns R, Danehy P and Peters C 2016 Multiparameter flowfield measurements in high-pressure, cryogenic environments using femtosecond lasers 32nd *AIAA Aerodynamic Measurement Technology and Ground Testing Conf.* AIAA Paper 2016-3246
[39] Pouya S, Van Rhijn A, Dantus M and Koochesfahani M 2014 Multi-photon molecular tagging velocimetry with femtosecond excitation (FemtoMTV) *Exp. Fluids* **55** 1791–8
[40] Koochesfahani M and Nocera D 2007 *Molecular Tagging Velocimetry Handbook of Experimental Fluid Dynamics*, ed J Foss, C Tropea and A Yarin (New York: Springer) ch 5.4
[41] Hammer P, Pouya S, Naguib A and Koochesfahani M 2013 A multitime-delay approach for correction of the inherent error in single-component molecular tagging velocimetry *Meas. Sci. Technol.* **24** 105302
[42] Burns R A, Danehy P M, Halls B R and Jiang N 2016 Femtosecond laser electronic excitation tagging velocimetry in a transonic, cryogenic wind tunnel *AIAA J.* **55** 680–5
[43] Sijtsema N M, Dam N J, Klein-Douwel R J H and Ter Meulen J J 2002 Air photolysis and recombination tracking: a new molecular tagging velocimetry scheme *AIAA J.* **40** 1061–4
[44] Lempert W R, Jiang N, Sethuram S and Samimy M 2002 Molecular tagging velocimetry measurements in supersonic microjets *AIAA J.* **40** 1065–70
[45] Andre M A, Bardet P M, Burns R A and Danehy P M 2016 Development of hydroxyl tagging velocimetry for low velocity flows *32nd AIAA Aerodynamic Measurement Technology and Ground Testing Conf.* (*Washington, DC*) (https://doi.org/10.2514/6.2016-3247)
[46] Kulatilaka W, Gord J and Roy S 2014 femtosecond two-photon lif imaging of atomic species using a frequency-quadrupled Ti:sapphire laser *Appl. Phys.* B **116** 7–13
[47] Zhang Y, Danehy P M and Miles R B 2018 Femtosecond laser tagging in 1, 1, 1, 2-tetrafluoroethane with trace quantities of air *2018 AIAA Aerospace Sciences Meeting* p 1027
[48] DeLuca N J, Miles R B, Jiang N, Kulatilaka W D, Patnaik A K and Gord J R 2017 FLEET velocimetry for combustion and flow diagnostics *Appl. Opt.* **56** 8632–8